1
Observing global properties of time-delayed feedback control in electronic circuits

Hartmut Benner, Chol-Ung Choe, Klaus Höhne, Clemens von Loewenich, Hiroyuki Shirahama, and Wolfram Just

1.1
Introduction

Control of complex and chaotic behaviour has been one of the most rapidly developing topics in applied nonlinear science for more than one decade (cf. [1] and references therein). Contrary to traditional control schemes which have been developed by engineers and applied mathematicians for more than half a century the emphasis of non-invasive methods has lead to new concepts like time-delayed feedback techniques [2]. Such a method has proven to be very useful in applications, in particular in experiments in physics, chemistry or bioscience. Meanwhile the control mechanism has been understood from the theoretical point of view, as far as linear aspects of the control scheme are concerned (cf. e.g. [3]). But there is still considerable lack of knowledge from the global point of view, e.g. with respect to stability of the control scheme under external perturbations or the structure of basins of attraction of the controlled state. Such basins are of utmost importance in experimental realisations since their size determines the accessibility of the target state. Unfortunately, time-delayed feedback control turns the dynamical system of interest into a differential-difference system and thus changes the structure of the underlying phase space considerably. Even if the original system has a quite simple structure, e.g. a low-dimensional phase space where only a few degrees of freedom are relevant, the phase space becomes infinite-dimensional by the application of time-delayed feedback since the whole history of the state enters the dynamics as well [4]. Such a feature makes the investigation of global phase space properties a difficult task even if one just wants to visualise high-dimensional basins of attraction, not to mention a systematic theoretical study.

Here we are going to study global features of time-delayed feedback control for two different setups using electronic circuit experiments. In section 1.2 extended time-delayed feedback control is investigated [5]. We focus in particular on the reduction of basins of attraction which is related with discon-

Titel. Author(s)

ISBN: 3-527-XXXXX-X

tinuous transitions at the control boundaries, a phenomenon which is already predicted by general bifurcation theory. Consequences of such a phenomenon for experiments are illustrated. Section 1.3 deals with an extension of time-delayed feedback control employing an unstable control loop to improve the control performance of time-delayed feedback control [6]. We investigate how different types of coupling of the control force affects the basins of attraction and thus may improve the control performance from a global perspective.

1.2 Discontinuous transitions for extended time-delayed feedback control

Time-delayed feedback methods are based on the measurement of a signal $s(t)$. The control force is generated from a time-delayed difference $s(t) - s(t - \tau)$. In order to keep such a scheme non-invasive the delay time τ is typically chosen to be the period of the target state. In order to improve the control performance filtering techniques in the frequency domain may be applied [5] so that the actual generation of the control force F reads

$$F(t) = K[s(t) - s(t - \tau)] + RF(t - \tau) \quad . \tag{1.1}$$

For filter parameter $R = 0$ the original Pyragas scheme is recovered where the control amplitude K yields one control parameter. The additional filter parameter R improves the control performance, in particular, when systems with fast time scales are considered. The control force is used to modulate an accessible parameter of the system. By adjustment of the two control parameters, K and R, successful stabilisation of the target state may be achieved. Of particular interest for our purpose will be the set of initial conditions for which control works successfully.

1.2.1 Theoretical considerations

Control performance of the extended scheme, Eq. (1.1), can be evaluated for quite general systems based on a linear stability analysis (cf. e.g. [7]). In particular, the control domain, i.e. the set of parameter values in the K–R control parameter plane for which control works successfully, shows generically a characteristic V-shape (cf. Fig. 1.1) when target states with an unstable negative Floquet multiplier are considered, e.g. unstable periodic orbits that have been generated via a period doubling cascade. The left-hand border of the control domain, the so-called lower control threshold, is connected with a period doubling bifurcation while the right-hand border of the domain is usually caused by a Hopf instability. While details of the control domain may depend

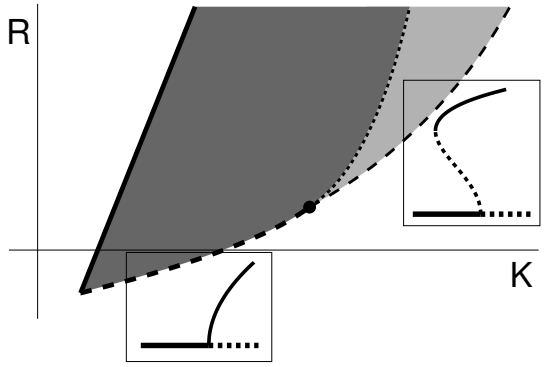

Table 1.1 Diagrammatic view of the control domain (dark and light grey-shaded) for extended time-delayed feedback control. Lower control threshold (solid line), upper control threshold (broken line), saddle node bifurcation of the delay-induced orbit (dotted line). The dot indicates a transition from continuous to discontinuous bifurcation (cf. insets for the bifurcation diagram). The corresponding region of bistability between the controlled orbit and the delay-induced motion is light grey-shaded.

on the particular system the overall picture coincides with the scenario just sketched (cf. e.g. [8–10] for further details).

The upper control threshold, i.e. the right-hand border of the control domain will be of interest for our purpose as Hopf bifurcations yield a generic mechanism to determine basin boundaries [11]. If the transition at the control boundary is continuous then a stable oscillating, quasiperiodic solution is generated beyond the upper control threshold. But for discontinuous transitions a completely different dynamical state is reached when leaving the control domain. Furthermore, the Hopf bifurcation is caused in such a case by a collision with a formerly unstable limit cycle (cf. insets in Fig. 1.1) which exists throughout the control domain. Within the control domain this unstable object gives rise to a finite basin of attraction. Furthermore, bistability and hysteresis are observed. In particular, the basin of attraction becomes small when the control boundary is approached. Thus a discontinuous transition is an indicator for small basins of attraction and the character of the instability is crucial for the global properties of the control system.

1.2.2 Experimental setup

We are going to demonstrate the relevance of such a mechanism by an electronic circuit experiment which has been performed recently [12]. A simple non-autonomous system is the nonlinear diode resonator sketched in Fig. 1.2. The circuit, which consists of an inductor (470μH), a resistor (51Ω) and three parallel diodes (1N4006) acting together as a nonlinear capacitor, is sinusoidally

driven at fixed frequency (340kHz), $U(t) = U_a \sin(2\pi\nu t)$. Without control the system undergoes a period doubling cascade to chaos on variation of the driving amplitude U_a. This scenario ensures for unstable periodic orbits with finite torsion so that these states are accessible to time-delayed feedback control [3]. We performed our experiments at $U_a = 4.5$V and choose the unstable period-one orbit as our target state. We measured the voltage at the resistor R and generated from this signal $s(t)$ our control force. The control loop employs multiple delay terms which exactly emulate the recursive form of Eq. (1.1). Finally the output of the control device was fed back to the driving voltage $U(t)$.

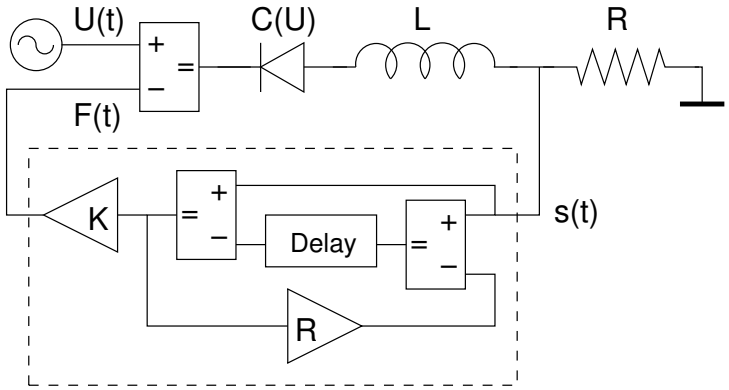

Table 1.2 Experimental setup of the nonlinear diode resonator with extended time-delayed feedback control device.

Having fixed the filter parameter R there exists a lower and an upper control threshold for successful control. At the lower threshold the unstable orbit becomes stable through an inverse period doubling cascade and the output signal $s(t)$ becomes finally periodic. At the upper control threshold the power spectrum develops side-bands. A Hopf bifurcation takes place which leads to a quasiperiodic state. Thus the scenario is in full accordance with the general theoretical considerations of the previous section.

1.2.3
Observation of bistability

Experimentally the Hopf bifurcation shows up most clearly in the frequency spectrum of the signal $s(t)$. Inside the control domain we observe one sharp line indicating the frequency of the controlled orbit. On increasing K a side-band frequency together with its harmonics occurs directly at the Hopf bifurcation (cf. Fig. 1.3). But this change happens discontinuously. When decreasing K this spectrum is maintained for a larger range until the system finally

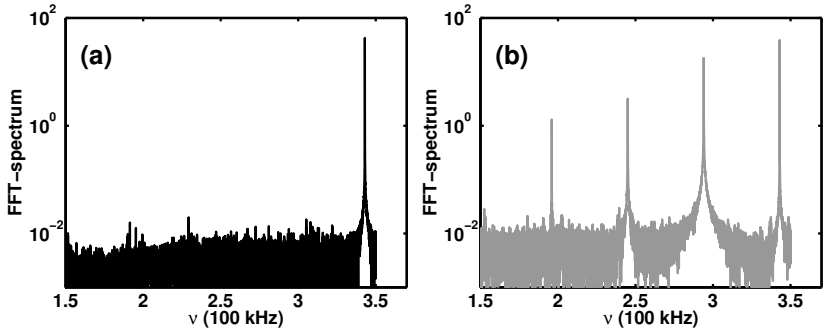

Table 1.3 Fourier spectrum of the measured signal at $K = 9.76$ and $R = 0.12$ for two different initial conditions: (a) controlled periodic orbit (adiabatic increase of the control amplitude), (b) delay-induced quasiperiodic state (adiabatic decrease of the control amplitude).

jumps back to the controlled state. This kind of hysteresis indicates that the observed Hopf bifurcation is subcritical and that a region of bistability between the controlled periodic orbit and a delay-induced quasiperiodic state occurs.

For the quantitative evaluation of the bistability we took the amplitude of the first side-band peak at about 290kHz. Figure 1.4 shows the dependence on the control amplitude when K is adiabatically increased, respectively decreased. Hysteresis and bistability is clearly visible with extremely sharp thresholds in K. At the right-hand threshold a subcritical Hopf instability takes place, i.e. a quasiperiodic peak with finite amplitude occurs in the

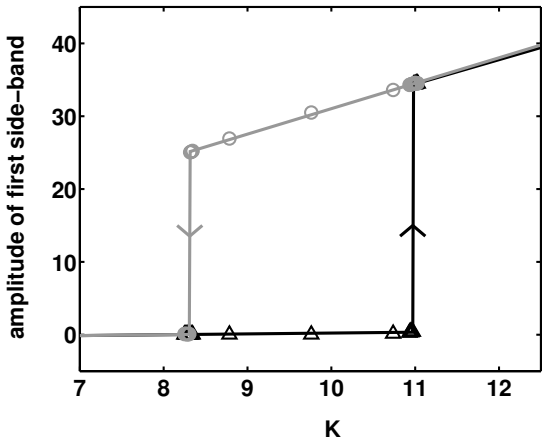

Table 1.4 Amplitude of the first side-band at 290 kHz vs. control amplitude K for $R = 0.12$. Triangles: increasing K, circles: decreasing K. (cf. Fig. 1.3 for corresponding Fourier spectra).

spectrum. The left-hand threshold, i.e. the discontinuous breakdown of the quasiperiodic state is caused by a saddle node bifurcation (cf. e.g. [11]).

Since the control domain and the just mentioned threshold values strongly depend on the filter parameter R we have probed the hysteresis for an accessible range $-0.25 < R < 0.25$. Figure 1.5 shows the corresponding thresholds in the K–R parameter plane. The lower threshold where control sets in and which is caused by the inverse flip bifurcation yields a straight line, in accordance with the theoretical prediction. No hysteresis was observed at this lower threshold. Thus the bifurcation is supercritical. At the upper control threshold we observe a subcritical Hopf bifurcation for all R values. The region of bistability which is bounded by the saddle node instability of the delay-induced quasiperiodic state accounts for about 30% of the whole control domain. Within the whole range of investigated parameter values the Hopf bifurcation at the upper boundary remained subcritical. No transition to supercritical behaviour was observed. Apart from this feature the results are in full accordance with the theoretical expectation described above (cf. Fig. 1.1).

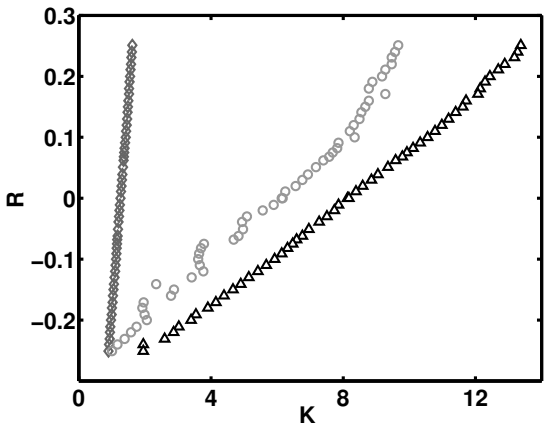

Table 1.5 Experimental results for the control thresholds in the K–R parameter plane. Diamonds: lower control threshold (supercritical flip bifurcation), triangles: upper control threshold (subcritical Hopf bifurcation), circles: collapse of the delay-induced quasiperiodic state (saddle node bifurcation).

1.2.4 Basin of attraction

As stated previously subcritical bifurcations pose severe constraints on the basin of attraction. We have analysed such a property by probing the corresponding basin of attraction directly in our experiment. Our setup was modified in a way that a short pulse could be added to the driving voltage

causing a perturbation to the stabilised orbit. A very short but strong pulse was applied at a fixed phase of the external periodic drive. Starting from the controlled state inside the bistable regime, we observed whether the system returned back to the controlled orbit or escaped to the quasiperiodic state. We made repeated experiments by varying systematically the control parameters as well as the width and the amplitude of the voltage pulse. As long as the strength of the pulse, i.e. the product of amplitude and width of the pulse does not exceed a critical value we find relaxation towards the periodic orbit. This critical strength gives a measure for the size of the basin of attraction. Results are shown in Fig. 1.6.

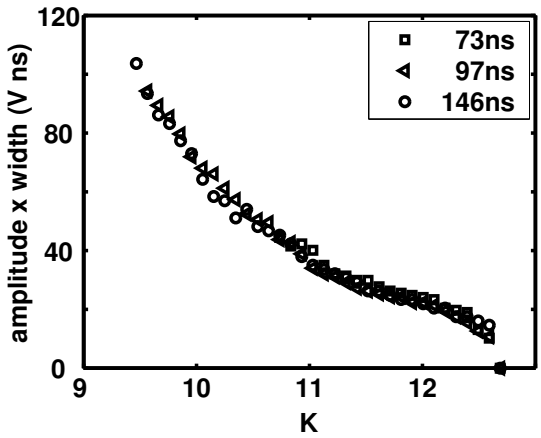

Table 1.6 Critical pulse strength in dependence on the control amplitude for different width of pulses at $R = 0.12$. Note that the modification of the experimental setup has slightly changed the system increasing the control thresholds by about 15%.

First of all we find that the critical pulse strength does not depend on the precise form of the pulse. On variation of the pulse width (2.5%, 3.3% and 5% of the period) the critical voltage amplitudes indicating the boundary of the basin of attraction scaled in the reciprocal way. Thus we obtained a nice data collapse and our experiment really probes for the basin of attraction. The size of the basin may be read off from the data displayed in Fig. 1.6.

Second, the critical pulse strength tends towards zero when the upper control threshold is approached. That property is in full accordance with the scenario of the subcritical Hopf bifurcation since the basin of attraction becomes small as well in that limit. Furthermore, the dependence of the pulse strength on K shows an S-shape characteristics which is expected for the size of the basin according to the theoretical prediction (cf. the upper inset in Fig. 1.1 and the corresponding normal form analysis, e.g. [13]). Thus we have striking experimental evidence that subcritical behaviour is a universal mechanism

which determines global features of time-delayed feedback control. Last but not least the data displayed in Fig. 1.6 indicate the sensitivity of the controlled system with respect to external perturbations and thus quantifies the degree of structural stability of the control scheme.

1.3 Controlling torsion-free unstable orbits

The second experimental example we are going to present refers to a control concept which is less straightforward than that in the previous case. It has been shown [3, 14] that only a certain class of periodic orbits characterised by a finite torsion can be stabilized by time-delayed feedback control. Such a topological constraint means that any unstable periodic orbit with an odd number of real Floquet multipliers larger than unity can never be stabilized by this method[1].

Different strategies have been suggested to overcome this constraint. For instance, the so-called rhythmic control [15] is based on the periodic modulation of the control signal with a period different from that of the orbit. This way the effect of torsion will be introduced artificially. Another way suggested recently [6] is based on the counter-intuitive concept to introduce an unstable degree of freedom into the control device. The key idea is to provide an even number of real Floquet multipliers by including an additional unstable degree of freedom in the feedback loop to overcome the limitation mentioned above. Bifurcation theory tells us that an even number of real unstable Floquet multipliers offers the possibility that, on variation of some bifurcation parameter, the corresponding Floquet branches may collide and undergo a Hopf bifurcation. This results in a complex conjugate pair of Floquet exponents (see Fig. 1.7). This way the missing torsion can be introduced via the additional unstable degree of freedom offered by the controller, and then the system becomes accessible again to time-delayed feedback control. A detailed discussion of this idea can be found in a previous chapter of the handbook. Both methods were successfully applied to control torsion-free unstable periodic orbits in numerical simulations, but real experimental applications have been missing so far.

A prominent paradigmatic system showing such torsion-free unstable orbits is the unstable van der Pol oscillator which is described by the following

1) In a recent reprint (arXiv:nlin.CD/0609056) Fiedler et al have pointed out that such a constraint does not apply for limit cycles in autonomous systems because time translation invariance allows for the occurrence of transcritical bifurcations. Actually, the proofs of the odd number limitation implicitly use the assumption that the underlying dynamics is subjected to a periodic drive.

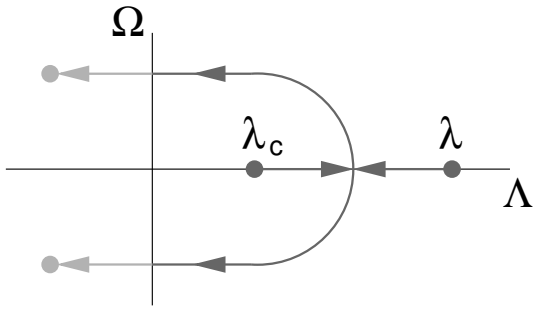

Table 1.7 Mechanism of time-delayed feedback control by means of an unstable controller. Λ and Ω are the real and imaginary parts of the Floquet exponent of the controlled system. The real Floquet exponents of the unstable system, λ, and of the unstable controller, λ_c , collide under the influence of the control force, and a Hopf bifurcation occurs.

equations of motion

$$\dot{x}(t) = -y(t) + \varepsilon x(t) + x^3(t)/3, \tag{1.2a}$$
$$\dot{y}(t) = x(t) \quad . \tag{1.2b}$$

Here, ε is the bifurcation parameter of system, and the time scale is normalized to the inverse oscillator frequency. Equation (1.2) differs from that for the conventional van der Pol oscillator merely by the sign of the nonlinear coefficient. For $\varepsilon < 0$, this equation has two coexisting solutions, a stable fixed point at the origin $x = y = 0$, and an unstable limit cycle with the period $\tau = 2\pi + \mathcal{O}(\varepsilon)$, amplitude $2\sqrt{-\varepsilon} + \mathcal{O}(\varepsilon)$, and a real positive Floquet exponent $\lambda = -\varepsilon + \mathcal{O}(\varepsilon^{3/2})$. For $\varepsilon > 0$ the limit cycle disappears, and the fixed point at the origin becomes unstable. Thus at $\varepsilon = 0$ we have a subcritical Hopf bifurcation. The real positive Floquet exponent indicates that the limit cycle is unstable and shows no torsion.

1.3.1 Applying the concept of an unstable controller

We assume that x is an observable accessible in experiment. To stabilize the unstable periodic orbit appearing for $\varepsilon < 0$ we consider the following control algorithm:

$$\dot{x}(t) = -y(t) + \varepsilon x(t) + x^3(t)/3 + w(t)f(x(t)) \tag{1.3a}$$
$$\dot{y}(t) = x(t) \tag{1.3b}$$
$$\dot{w}(t) = \lambda_c w(t) - K(x(t) - x(t-\tau))f(x(t)) \quad . \tag{1.3c}$$

The term $wf(x)$ in Eq. (1.3a) is the control signal perturbing the x-variable. The specific form of this coupling is given by the function $f(x)$ and will be

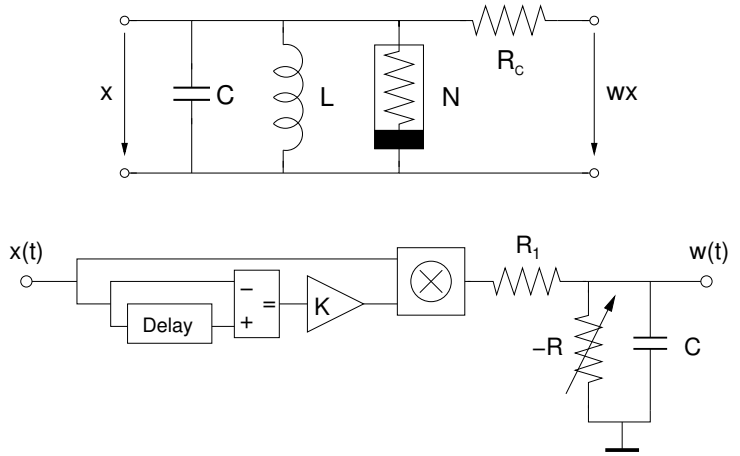

Table 1.8 Top: experimental implementation of unstable van der Pol oscillator by means of a parallel CLN resonator. The nonlinearity N is provided by a Chua diode. Bottom: design of the unstable controller described by Eq. (1.3)

specified later. Equation (1.3c) describes an unstable delayed feedback controller with $\lambda_c > 0$. Here w is the dynamical variable of the controller and K determines the feedback strength. Note that the control scheme does not change the solution of the free system corresponding to the unstable orbit of period τ, since for $x(t) = x(t-\tau)$ Eq. (1.3c) is satisfied by $w = 0$ and the control signal $w(t)f(x(t))$ in Eq. (1.3a) vanishes.

We just mention that in a recent article [16] Eq. (1.3) has been considered as a paradigm of a subcritical Hopf bifurcation showing an unstable torsion-free limit cycle. The possibility to stabilize such an orbit was explored both analytically and by means of numerical simulations, and successful control was achieved.

1.3.2 Experimental design of an unstable van der Pol oscillator

In order to probe the concept of an unstable controller in experiment we designed autonomous electronic circuits which could be mapped to Eq. (1.3). We first considered a serial LC oscillator with a cubic nonlinearity as had been suggested in [16]. The obvious idea to approximate the nonlinearity by a conventional Chua diode failed, because in such a circuit current and voltage were just interchanged with respect to the diode characteristics. However, a circuit with inductance, capacity, and nonlinearity in parallel connection (cf. Fig. 1.8) should overcome this problem and seemed to give a proper realization of our model Eq. (1.2). By means of a so-called 'negative resistor' the unstable controller was designed in a straightforward way choosing for

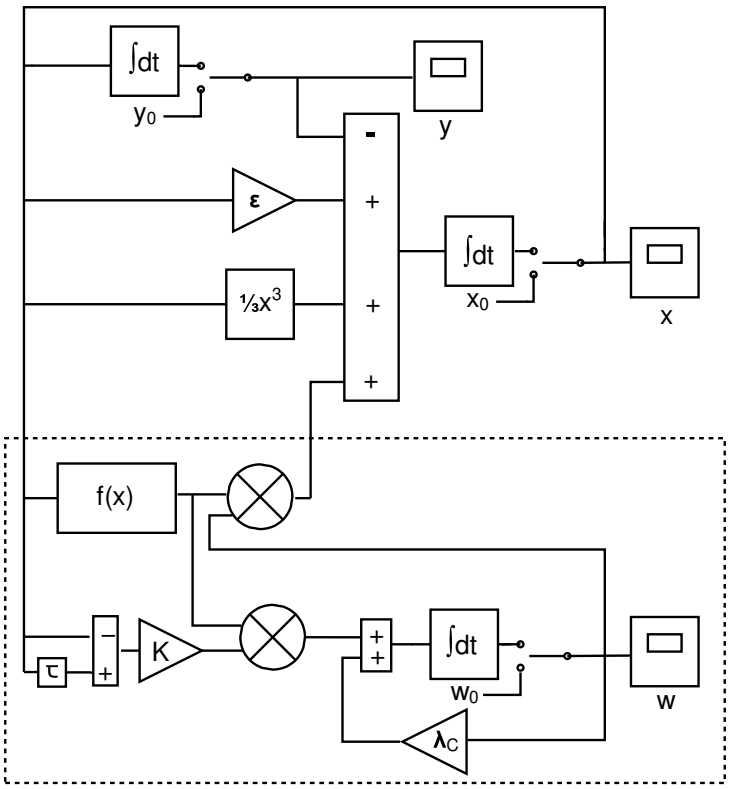

Table 1.9 Block diagram of the van der Pol oscillator with control loop (setup built from active components).

the coupling function $f(x)$ a simple linear one, $f(x) = x$. Nevertheless, our attempts to control such an electronic realization of the unstable van der Pol oscillator were not successful. Failure was obviously caused by parasitic properties of the components. For instance, we found that the internal resistance of the inductor L gave rise to a rather strong symmetry-breaking term which spoiled the model properties. Moreover, this type of setup did not yet allow to define the initial conditions of the system with sufficient accuracy.

In order to overcome these problems we finally decided to construct our model circuit merely from active components. So, Eq. (1.3) was designed step by step using operational amplifiers and integrated circuits. A block diagram of this setup is presented in Fig. 1.9. It includes the unstable controller as well as elements for defining the experimental initial conditions. The components at the top of Fig. 1.9 maps the relation $\dot{y} = x$. Then, by integrating x the variable y is obtained. The adder comprehends all terms contributing to $\dot{x}$, and x is again obtained by integration. The controller variable w is coupled to the

x-component, so the product of w and $f(x)$ is also included in the adder inputs, while the delay term and the intrinsic instability of w are generated by the loops at the bottom. The bifurcation parameter ε, the control amplitude K, and the positive exponent λ_c are simply determined by the gain of electronic amplifiers. For defining the initial conditions, we introduced switches parallel to each of the integrator outputs which generate the variables $x(t), y(t)$ and $w(t)$. These switches allowed to apply adjustable constant voltages x_0, y_0 and w_0, respectively. Thus, when switching on the system at $t = 0$, the variables $x(t)$ and $y(t)$ started from a well-defined state. At about one cycle later the feedback loop generating the control signal was switched on, simultaneously with the controller variable $w(t)$. Such a time-lag was necessary to obtain an appropriate delayed signal reflecting the dynamics of the uncontrolled system close to the initial state. Note that the control generally failed when the feedback is switched on earlier than one cycle or later than seven or eight cycles. This is understandable since in the former case a proper delay signal has not yet developed while in the latter case the unstable system has already escaped too far away from the target state.

1.3.3
Control coupling and basin of attraction

An essential result of our investigations was that the success of the unstable controller concept depends sensitively on the specific form of the coupling function $f(x)$. Our first choice for $f(x)$ followed the coupling suggested in [16]. The unstable degree of freedom, w, was coupled to the x-variable and, in turn, the delay term was coupled to the unstable controller w via a linear coupling $f(x) = x$ (cf. Eq. (1.3c)). In numerical simulations such a coupling had turned out to be essential for the control performance [16]. When applying this coupling scheme to our experiment, however, it failed for a large range of initial conditions. Figure 1.10 reflects a typical experimental situation. We chose the bifurcation parameter $\epsilon = -0.1$, the control amplitude $K = 0.3$, and $y(0)$ and $w(0)$ were set to zero, while $x(0)$ was set to 0.2V. We repeated the control experiment several times with the same set of parameters. In most cases the controller variable $w(t)$ immediately escaped to infinity while $x(t)$, after some irregular transients, settled either in the stable fixed point (cf. Fig. 1.10, l.h.s. column) or ended up in a high amplitude oscillatory state which meets the saturation limits of the operational amplifiers. In some cases, however, for the very same set of parameters we also achieved successful control (cf. Fig. 1.10, r.h.s. column), which, in fact, represents the first experimental evidence approving the concept of an unstable controller. The low success rate indicated that the method is rather sensitive to perturbations introduced by noise and by the irregular motion of the uncontrolled system

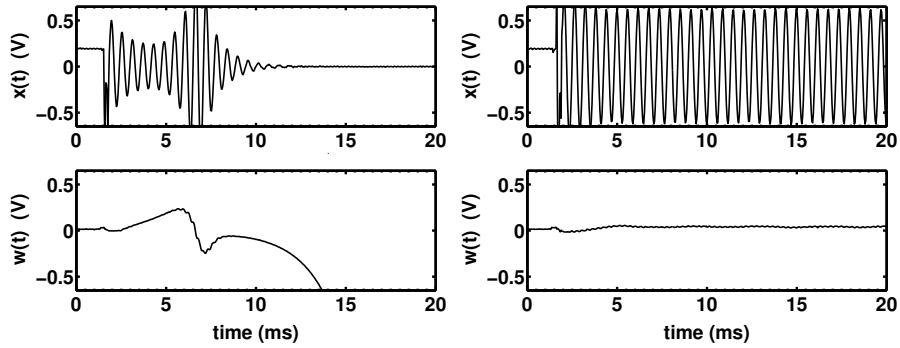

Table 1.10 Two attempts to control a torsion-free unstable orbit with linear coupling $f(x) = x$. Time series of $x(t)$ and $w(t)$ for the same set of initial conditions: $\varepsilon = -0.1$, $K = 0.3$, $x(0) = 0.2$V, $y(0) = w(0) = 0$V. Left: relaxation towards the trivial fixed point with divergent control variable $w(t)$. Right: Successful non-invasive stabilisation of the unstable periodic orbit.

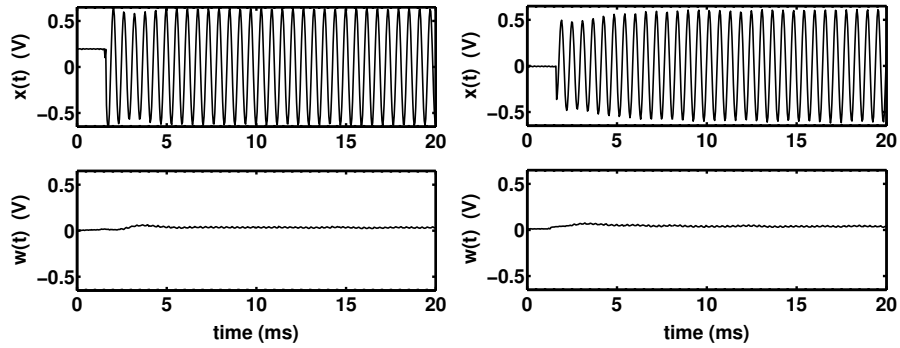

Table 1.11 Successful control of torsion-free unstable orbits with $f(x) = \text{sign}(x)$, $\varepsilon = -0.1$, $K = 0.3$ and $y(0) = w(0) = 0$V for different initial conditions: $x(0) = 0.2$V (left) and $x(0) = 0$V (right).

during the starting phase. Such missing robustness is generally considered a serious drawback for practical applications.

However, it turned out that the low success rate could be improved considerably by changing the control function. When replacing the linear coupling $f(x) = x$ by a sigmodal one, e.g. $f(x) = \text{sign}(x)$ or $f(x) = \tanh(\beta x)$, $\beta \gg 1$, the situation changed dramatically. Technically such a modification of the coupling could be easily implemented by means of an operational amplifier acting as a comparator. After such an implementation successful control could be achieved for a larger range of initial conditions with a success rate of almost 100% (cf. Fig. 1.11).

A quantitative estimate of the success of control was obtained by varying both control amplitude and initial conditions. For the case of linear coupling

optimal control performance (for $\varepsilon = -0.1$) was obtained at $K = 0.15$. We set $x(0)$ and $w(0)$ to zero and increased $y(0)$ from 0 to 1V in steps of 0.01V. For each set of initial values we repeated the control experiment about 100 times. The part of successful attempts is shown in a histogram (cf. Fig.1.12). For linear coupling successful control was only achieved for $y(0)$ values from the neighborhood of the unstable orbit which is indicated by the dashed line at 0.63V. For the case of a sigmodal coupling optimal control was observed at $K = 0.35$, and the control regime was much larger than in the linear case. Accordingly we also obtained a much larger 'basin of attraction' for the controlled orbit which now covers the full $y(0)$ range from 0 to 0.8V yielding a success rate of almost 100%. At present we may only speculate about the mechanism for such a strong improvement. It is probably related to the limitation of the control force for strongly fluctuating x-transients during the onset of control. Without such a limitation large x-fluctuations might destroy the control by 'overshooting'.

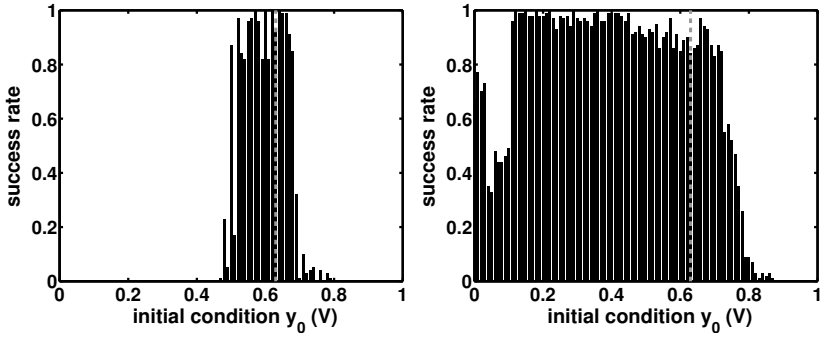

Table 1.12 'Basins of attraction' for different control couplings. L.h.s.: linear coupling $f(x) = x$, $K = 0.15$ (while $\varepsilon = -0.1$, $x(0) = w(0) = 0$V). r.h.s.: sigmodal coupling $f(x) = \mathrm{sign}(x)$, $K = 0.35$. Location of the unstable orbit is indicated by dashed line.

1.4 Conclusions

Time-delayed feedback control has been investigated for two different setups with regards to the global control performance. In particular, basins of attraction have been probed in electronic circuit experiments. Extended time-delayed feedback control schemes were investigated in section 1.2. Reduced basins of attraction and reduced structural stability have been measured which were caused by discontinuous transitions at control thresholds. Thus, a universal mechanism, well known in bifurcation theory, has shown its relevance in electronic circuit experiments. Section 1.3 dealt with the implementation

of an unstable controller to stabilize torsion-free unstable periodic orbits that were generated in a subcritical Hopf bifurcation. The improvement of the control performance by changing the coupling scheme of the control force was demonstrated and a considerable enlargement of basins of attraction has been observed.

Some caution should be in place when using the term 'basin of attraction'. Since we were dealing with delay systems their dynamics is determined by previous states as well. Accordingly, the proper basin of attraction does not only depend on the actual values of the degrees of freedom, e.g. on initial conditions when the control is switched on, but also on the recorded delay states which determine the control force. When probing the basin of attraction in our experiment on the diode resonator in the section 1.2.4 the initial state was just the controlled orbit. The stability of this state in some neighborhood was probed by application of small perturbations which had even been synchronized with the phase of the external drive. Thus, all perturbations started from a state with a common history. Such a procedure may be considered as a finite dimensional cross section in the infinite-dimensional phase space of the delay system. In practical applications, however, one is often less interested in the stability of the controlled state against perturbations once the system has settled on it. The problem how to reach the controlled state in the most efficient way is usually of more interest. Therefore, we have chosen in section 1.3.3 a different type of approach to probe the global control performance. Here, control was switched on skipping a transient and the history of the dynamics was taken from the uncontrolled motion. Tiny fluctuations may amplify during the transient and we ended up with a probability distribution for successful control. Thus, the distributions reflect implicitly the size of the basin in a rather intricate way. Above all, such an approach seems to have a more direct relevance for real control experiments, although a direct link to theoretical considerations is more difficult to establish.

The experimental study is still in progress, and further systematic investigations on global properties are necessary. In particular, the effect of the specific form of control coupling on the control performance will be of major importance from the viewpoint of practical applications. Even now it is already clear that in systems without torsion the idea of the unstable controller does work and - for an appropriate type of coupling - results in robust time-delayed feedback control suitable for practical applications.

Bibliography

1 *Handbook of Chaos Control*, edited by H. G. Schuster (Wiley–VCH, Berlin, 1999).

2 K. Pyragas, *Continuous control of chaos by self-controlling feedback*, Phys. Lett. A **170**, 421 (1992).

3 W. Just, T. Bernard, M. Ostheimer, E. Reibold, and H. Benner, *Mechanism of time-delayed feedback control*, Phys. Rev. Lett. **78**, 203 (1997).

4 J. K. Hale and S. M. Verduyn Lunel, *Introduction to Functional Differential Equations* (Springer, New York, 1993).

5 J. E. S. Socolar, D. W. Sukow, and D. J. Gauthier, *Stabilizing unstable periodic orbits in fast dynamical systems*, Phys. Rev. E **50**, 3245 (1994).

6 K. Pyragas, *Control of Chaos via an Unstable Delayed Feedback Controller*, Phys. Rev. Lett. **86**, 2265 (2001).

7 W. Just, E. Reibold, H. Benner, K. Kacperski, F. Fronczak, and J. Hołyst, *Limits of time-delayed feedback control*, Phys. Lett. A **254**, 158 (1999).

8 J. E. S. Socolar and D. J. Gauthier, *Analysis and comparison of multiple-delay schemes for controlling unstable fixed points of discrete maps*, Phys. Rev. E **57**, 6589 (1998).

9 W. Just, E. Reibold, K. Kacperski, P. Fronczak, J. Hołyst, and H. Benner, *Influence of stable Floquet exponents on time-delayed feedback control*, Phys. Rev. E **61**, 5045 (2000).

10 O. Beck, A. Amann, E. Schöll, J. E. S. Socolar, and W. Just, *Comparison of time-delayed feedback schemes for spatio-temporal control of chaos in a reaction-diffusion system with global coupling*, Phys. Rev. E **66**, 016213 (2002).

11 J. Guckenheimer and P. Holmes, *Nonlinear Oscillations, Dynamical Systems, and Bifurcations of Vector Fields* (Springer, New York, 1986).

12 C. v. Loewenich, H. Benner, and W. Just, *Experimental relevance of global properties of time-delayed feedback control*, Phys. Rev. Lett. **93**, 174101 (2004).

13 W. Just, H. Benner, and C. v. Loewenich, *On global properties of time-delayed feedback control: weakly nonlinear analysis*, Physica D **199**, 33 (2004).

14 H. Nakajima, *On analytical properties of delayed feedback control of chaos*, Phys. Lett. A **232**, 207 (1997).

15 H. G. Schuster and M. B. Stemmler, *Control of chaos by oscillating feedback*, Phys. Rev. E **56**, 6410 (1997).

16 K. Pyragas, V. Pyragas, and H. Benner, *Delayed feedback control of dynamical systems at a subcritical Hopf bifurcation*, Phys. Rev. E **70**, 056222 (2004).

Index

Titel. Author(s)

ISBN: 3-527-XXXXX-X